2023年12月 矿 床 地 质 第42卷 第6期
December，2023 MINERAL DEPOSITS 42（6）：1214~1228

文章编号：0258-7106（2023）06-1214-15 Doi: 10. 16111/j. 0258-7106. 2023. 06. 008

岩浆-热液成矿系统中铁同位素地球化学研究现状*

王续文，李宇轩，安 芳**

（大陆动力学国家重点实验室 西北大学地质学系，陕西 西安 710069）

摘 要 铁元素是岩浆-热液成矿系统中参与成矿的重要金属元素之一，岩浆-热液矿床中富铁矿物（黄铁矿、磁铁矿、黄铜矿、磁黄铁矿、斑铜矿、毒砂、菱铁矿）的 $\delta^{56}Fe$ 值变化较大（−2.07‰~+1.58‰），指示铁同位素在岩浆演化、流体出溶和热液演化过程中均存在明显的分馏，因此，在约束岩浆-热液成矿系统中成矿金属的迁移-富集-沉淀过程和示踪成矿物质来源方面具有巨大的应用潜力。通过整理和分析前人研究资料，文章总结了岩浆-热液成矿系统岩浆演化、流体出溶和热液演化过程中铁同位素地球化学行为的研究现状。岩浆演化过程中铁同位素会发生显著分馏，如部分熔融过程中，熔体相比残余固相富集重铁同位素；矿物分离结晶会引起残余熔体铁同位素组成的变化，主要受含 Fe^{2+} 或 Fe^{3+} 矿物结晶的影响，如磁铁矿分离结晶会导致残余熔体铁同位素组成变轻，总体反映岩浆氧化还原状态对铁同位素分馏的主要控制作用，因此，含矿岩体铁同位素组成及其变化可用于确定岩浆的氧化还原状态。流体出溶是含矿岩浆演化成为岩浆热液矿床的关键过程，出溶流体相对于母岩富集轻铁同位素，但实验研究表明出溶流体铁同位素组成可能受其中铁的迁移形式、与流体平衡的含 Fe^{2+} 或 Fe^{3+} 矿物的比例、相分离和流体混合等多种因素影响。热液演化过程中，含铁热液矿物沉淀会引起流体铁同位素组成的变化，磁铁矿沉淀会导致流体富集轻铁同位素，而含铁硫化物（如磁黄铁矿）沉淀则会使得流体逐渐富集重铁同位素，显示热液流体氧化还原状态对铁同位素分馏的控制作用。由于黄铜矿被认为可以有效记录流体的铁同位素组成，其铁同位素值被用于区分热液流体氧化还原状态。铁元素作为岩浆-热液成矿系统中直接参与成矿的元素，为直接示踪成矿物质来源提供了可能性，然而，岩浆演化、流体出溶和热液演化过程中铁同位素的明显分馏，导致利用铁同位素示踪成矿物质来源的特殊性。进一步明确流体出溶、热液演化等地质过程中的分馏规律，是利用铁同位素示踪成矿物质来源的关键。

关键词 Fe同位素；岩浆-热液成矿系统；地球化学行为；应用研究现状

中图分类号：P618.31 **文献标志码**：A

Status and progress on geochemical behavior of iron isotope in magmatic-hydrothermal system

WANG XuWen, LI YuXuan and AN Fang

(State Key Laboratory of Continental Dynamics, Department of Geology, Northwest University, Xi'an 710069, Shaanxi, China)

Abstract

Iron element is one of the important metal elements involved in mineralization in the magmatic-hydrothermal metallogenic system. The $\delta^{56}Fe$ values of iron-rich minerals (pyrite, magnetite, chalcopyrite, pyrrhotite, bornite, arsenopyrite, siderite) in magmatic-hydrothermal deposits vary considerably(−2.07‰~+1.58‰), indicating that the iron isotope has obvious fractionation during the magmatic evolution, fluid exsolution and hydrothermal evolution, therefore, it has great application potential in constraining the migration-enrichment-precipitation process of ore-forming metals and tracing the source of ore-forming materials in the magmatic-hydrothermal metallogenic system. Based on sorting out and analyzing the data of previous studies, this paper summarizes the

http://www.kcdz.ac.cn/

* 本文得到国家自然科学基金项目（编号：42273062、42130102）和西北大学地质学系科研基金项目的联合资助

第一作者简介 王续文，男，2000年生，硕士研究生，地质学专业。Email：2382374990@qq.com

** 通讯作者 安 芳，女，1984年生，教授，主要从事矿床学、矿床地球化学方面研究工作。Email：anfang_china@163.com

收稿日期 2023-02-09；改回日期 2023-09-23。秦思婷编辑。

research status of iron isotope geochemical behavior in magmatic evolution, fluid exsolution and hydrothermal evolution of magmatic-hydrothermal metallogenic system. The iron isotope will undergo significant fractionation in the process of magmatic evolution, and the melt phase is enriched in heavy iron isotope than the residual solid phase during partial melting; the iron isotope composition of the residual melt is changed due to the separation and crystallization of minerals, which are mainly affected by the crystallization of minerals containing Fe^{2+} or Fe^{3+}, for example, separation and crystallization of magnetite will lead to enrichment of light iron isotope composition in the residual melt, which generally reflects the main control of the redox state of magma on the fractionation of iron isotopes. Therefore, the composition and variation of iron isotope in ore-bearing rocks can be used to determine the redox state of magma. Fluid exsolution is a key process in the evolution of ore-bearing magma into magmatic hydrothermal deposits, the exsolution fluid is rich in light iron isotope relative to the host rock, however, the experimental studies show that the iron isotope composition of the exsolution fluid may be affected by many factors, such as the migration form of iron, the proportion of Fe^{2+} or Fe^{3+} containing minerals in equilibrium with the fluid, the phase separation and the fluid mixing. During the hydrothermal evolution, the precipitation of iron bearing hydrothermal minerals will cause changes in the iron isotope composition of the fluid, the magnetite precipitation will cause the fluid to enrich the light iron isotope, and the precipitation of iron-bearing sulfides (such as pyrrhotite) makes the fluid gradually enrich the heavy iron isotopes, which shows that the redox state of hydrothermal fluid controls the fractionation of iron isotopes. Since chalcopyrite is considered to be able to effectively record the iron isotope composition of the fluid, its iron isotope value is used to distinguish the redox state of hydrothermal fluid. As an element directly involved in mineralization in the magmatic hydrothermal metallogenic system, iron provides a possibility for direct tracing of the source of ore-forming materials, however, the obvious fractionation of iron isotopes in magmatic evolution, fluid dissolution and hydrothermal evolution leads to the particularity of tracing the source of ore-forming materials with iron isotopes. It is the key to trace the source of ore-forming materials by iron isotopes to further clarify the fractionation rules in the geological processes such as fluid dissolution and hydrothermal evolution.

Key words: Fe isotope, magmatic-hydrothermal metallogenic system, geochemical behavior, application research status

铁是太阳系中丰度最高的元素之一,也是地球内分布最多、最广泛的金属元素。铁有^{54}Fe、^{56}Fe、^{57}Fe和^{58}Fe四个稳定同位素,其稳定同位素组成通常用$\delta^{56}Fe$或$\delta^{57}Fe$来表示,代表样品中$^{56}Fe/^{54}Fe$、$^{57}Fe/^{54}Fe$比值相对于国际标准物质IRMM-014的千分偏差,对于质量分馏而言,$\delta^{56}Fe=0.678\delta^{57}Fe$。近年来,随着多接收电感耦合等离子体质谱(MC-ICP-MS)测试技术的发展,实现了铁同位素的高精度测定,为开展铁同位素地球化学研究提供了重要技术手段,使得铁同位素在宇宙科学、地球科学、环境科学等多个领域得到了广泛应用(Anbar, 2004;2007;Beard et al., 2004a;Dauphas et al., 2006;Johnson et al., 2008;王跃等, 2012;何永胜等, 2015;朱祥坤等, 2016)。

在地球科学领域,随着近年来研究数据的积累,各种地质储库、多种岩浆矿物、岩石和热液流体/矿物的铁同位素组成和变化范围已陆续被总结出来(王跃等, 2012;何永胜等, 2015;朱祥坤等, 2016),理论计算和实验研究也获得了部分矿物-熔体、矿物-流体和矿物-矿物的铁同位素平衡分馏系数(Hill et al., 2010;Polyakov et al., 2011;Saunier et al., 2011;Syverson et al., 2013; 2017;Wu et al., 2017)。以上研究成果极大促进了铁同位素地质应用的发展,目前铁同位素主要应用于生物过程(Beard et al., 2003;Rouxel et al., 2018)、环境变化(Zhu et al., 2000;Xiang et al., 2020)、岩浆演化(Du et al., 2017;Li et al., 2020)等领域。在矿床学中的应用主要集中在条带状铁建造(Li et al., 2013;Yang et al., 2019;Zhu et al., 2019;Huang et al., 2021)、海底热液成矿系统(高兆富等, 2016;Rouxel et al., 2018;高兆富等, 2020;Wang et al., 2020)、岩浆成矿系统(Liu et al., 2014;Ding et al., 2019;Troll et al., 2019)、岩浆-热液成矿系

http://www.kcdz.ac.cn/

统(Wang et al., 2011; Wawryk et al., 2017; He et al., 2020)、其他热液成矿系统(Liu et al., 2021; Zhang et al., 2021),以及矿床的表生氧化作用等方面(Cheng et al., 2015),上述研究表明铁同位素在示踪矿床成矿物质来源和约束矿床成因方面具有极大潜力,并为铁同位素矿床学应用研究积累了诸多数据。

近年对岩浆-热液成矿系统铁同位素组成和示踪应用的数据在逐渐积累,已开展研究的矿床类型包括斑岩型钨锡矿床(Wawryk et al., 2015)、斑岩型铜矿床(Graham et al., 2004; Li et al., 2010; Wawryk et al., 2015; Li et al., 2018; Zhu et al., 2018; Zhang et al., 2021)、矽卡岩型矿床(Graham et al., 2004; 王跃, 2011; Pi et al., 2015; Zhu et al., 2016; Bao et al., 2021; Wang et al., 2021; 陈福川等, 2022)以及部分岩浆热液型金矿床(Zheng et al., 2021)。这些研究分析了岩浆-热液矿床中主要含铁矿物(黄铁矿、磁铁矿、磁黄铁矿、黄铜矿等)的铁同位素组成,结果显示,岩浆-热液矿床中含铁矿物的δ^{56}Fe值变化较大(−2.07‰~+1.58‰),且不同类型矿床的铁同位素组成和变化规律存在一定差异(图1a~d),表明铁同位素对岩浆-热液矿床的成矿过程比较敏感,在示踪成矿过程(包括岩浆性质、流体出溶、成矿流体演化)和成矿物质来源方面具有潜力(Gagnevin et al., 2012; Pi et al., 2015; Wang et al., 2015; Wawryk et al., 2015; Zhu et al., 2016; Li et al., 2018; He et al., 2020; 韦刚健等, 2022)。在前人大量研究基础上,本文总结了不同类型岩浆-热液矿床的铁同位素组成,对岩浆-热液成矿系统岩浆演化、流体出溶、热液演化过程中铁同位素的地球化学行为,以及铁同位素在示踪物质来源方面的应用研究现状进行了综述。

1 不同类型岩浆-热液矿床的铁同位素组成及变化规律

了解不同类型岩浆-热液矿床的铁同位素组成及其变化规律,是开展岩浆-热液系统中铁同位素地球化学行为研究的前提。笔者统计了矽卡岩型、斑岩型铜-钼/金矿、斑岩型钨锡矿和岩浆热液型金矿等岩浆-热液矿床中主要含铁矿物(黄铁矿、磁黄铁矿、磁铁矿、黄铜矿、斑铜矿、毒砂以及菱铁矿)的铁同位素组成(图1a~d),以更好地显示各类岩浆-热液矿床的铁同位素组成、变化规律,以及不同类型矿床铁同位素组成的差异。

岩浆热液型金矿床主要为由含金岩浆热液演化形成的一类矿床,例如辽东半岛的五龙金矿,矿区的主要成矿岩体为花岗岩(Zheng et al., 2021),闪长岩

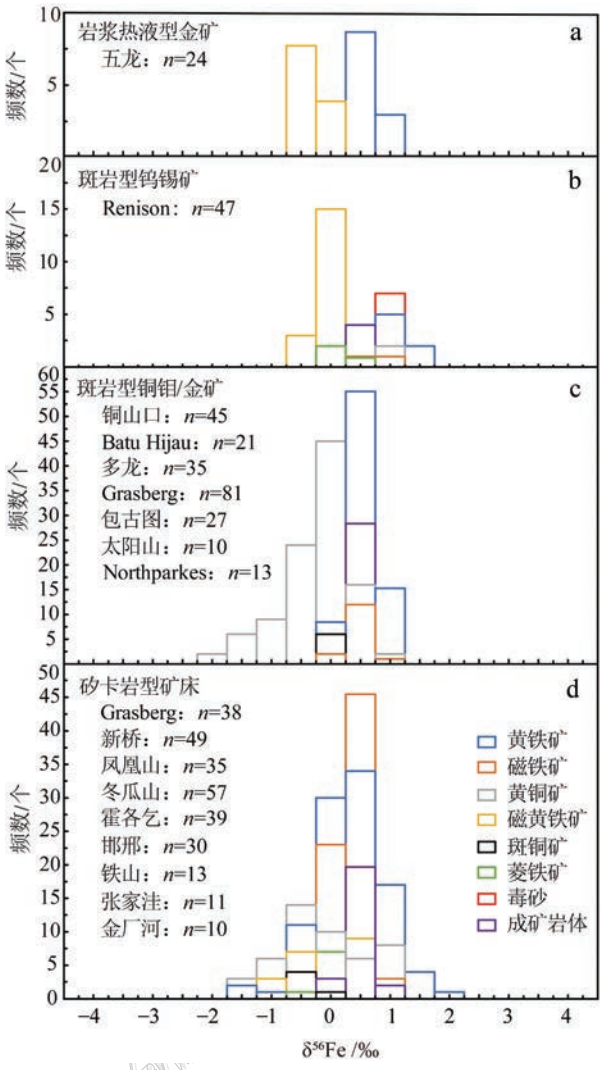

图1 不同类型岩浆-热液矿床含铁矿物和成矿岩体铁同位素组成

岩浆热液型金矿床据Zheng et al., 2021; 斑岩型钨锡矿床据Wawryk et al., 2015; 斑岩型铜钼/金矿床据Graham et al., 2004; Li et al., 2010; Wawryk et al., 2017; Li et al., 2018; Zhu et al., 2018; He et al., 2020; Zhang et al., 2021; 矽卡岩型矿床据Graham et al., 2004; 王跃, 2011; Pi et al., 2015; Zhu et al., 2016; Bao et al., 2021; Wang et al., 2021; 陈福川等, 2022

Fig.1 Iron isotope composition of iron-bearing minerals and ore-forming rocks in different types of magmatic-hydrothermal deposits

Data of magmatic hydrothermal gold deposits after Zheng et al., 2021; Porphyry Sn-W deposits after Wawryk et al., 2015; Porphyry Cu-Mo/Au deposits after Graham et al., 2004; Li et al., 2010; Wawryk et al., 2017; Li et al., 2018; Zhu et al., 2018; He et al., 2020; Zhang et al., 2021; Skarn deposits after Graham et al., 2004; Wang, 2011; Pi et al., 2015; Zhu et al., 2016; Bao et al., 2021; Wang et al., 2021; Chen et al., 2022

脉在空间上与含金石英-硫化物脉相关。矿床中含铁热液矿物为黄铁矿和磁黄铁矿,自然金通常以小型复合包裹体(约5~60 μm)的形式出现在黄铁矿、磁黄铁矿和石英中(Zheng et al., 2021)。其中,黄铁矿变化范围为0~1.0‰,而磁黄铁矿的δ^{56}Fe值均显示为负值(−1.0‰~0)(图1a)。

澳大利亚塔斯马尼亚岛西部Renison斑岩型钨锡矿床的成矿岩体为成分从二长花岗岩到碱长花岗岩不等的S型花岗岩(Wawryk et al., 2015),成矿岩体的δ^{56}Fe值集中于0~0.5‰;矿床中的磁铁矿极少,铁矿物以磁黄铁矿为主,黄铁矿、毒砂和黄铜矿为辅,另有少量菱铁矿,其中磁铁矿δ^{56}Fe值为0.5‰~1.0‰,磁黄铁矿均表现为负δ^{56}Fe值(−1.0‰~0),毒砂δ^{56}Fe值为0.5‰~1.0‰,黄铁矿(0.5‰~1.5‰)和黄铜矿(0~1.0‰)也均以正值为主,但相对毒砂变化范围较大,菱铁矿δ^{56}Fe值则分布于−0.5‰~+1.0‰(图1b)。

斑岩型铜钼/金矿床在空间和成因上主要和钙碱系列的中酸性斑岩侵入体有关(Li et al., 2010; 2018; Wawryk et al., 2017; Zhu et al., 2018; He et al., 2020; Zhang L et al., 2021; Zhang Y W et al., 2021),成矿岩体的δ^{56}Fe值集中分布于0~0.5‰;矿床中磁铁矿的δ^{56}Fe值变化范围为−0.5‰~+1.0‰。含铁硫化物矿物以黄铜矿、黄铁矿为主,含有少量斑铜矿,黄铜矿δ^{56}Fe值变化范围较大,在−2.5‰~+1.0‰之间;黄铁矿δ^{56}Fe值(−0.5‰~+1.5‰)变化范围较黄铜矿小,斑铜矿δ^{56}Fe值则集中分布于−0.5‰~0(图1c)。

矽卡岩型铁矿床常与石英闪长岩、闪长岩有关(Zhu et al., 2016; Wang et al., 2021),铜矿床大多和花岗闪长岩、石英二长岩有关,但不同类型矿床成矿岩体的δ^{56}Fe值变化不大,集中分布在0~0.5‰之间,少数为负值(王跃, 2011);磁铁矿在矽卡岩型矿床含矿岩体和矽卡岩期广泛分布,其δ^{56}Fe值变化范围为−0.5‰~+1.0‰;石英-硫化物期以形成黄铁矿、黄铜矿、磁黄铁矿等铁矿物为主,另有少量斑铜矿和菱铁矿,其中,黄铁矿δ^{56}Fe变化范围较大,为−2.0‰~+2.0‰;黄铜矿较黄铁矿含量低,但变化范围依旧很大(−2‰~+1.0‰);磁黄铁矿δ^{56}Fe值为−1.5‰~+1‰,斑铜矿和菱铁矿δ^{56}Fe值为−1.0‰~0(图1d)。

以上不同类型岩浆-热液矿床铁同位素组成及变化规律表明,在岩浆-热液系统岩浆演化、流体出溶和热液演化过程中,铁同位素在矿物-熔体、流体-熔体、流体-矿物和矿物-矿物间均存在不同程度的分馏,为利用铁同位素示踪岩浆-热液成矿过程带来了机遇。然而,了解以上地质过程中铁同位素的分馏规律和控制因素,是对具体矿床的铁同位素数据做出解释,并发展铁同位素示踪模型的关键。

2　岩浆-热液成矿系统中铁同位素的地球化学行为

岩浆-热液成矿系统的成矿潜力取决于成矿岩浆的起源和演化,流体出溶是含矿岩浆能够演化为岩浆热液矿床的关键过程,而热液演化过程则决定着矿床的类型和分布特征(Wilkinson, 2013)。本文总结了岩浆-热液成矿系统岩浆演化、流体出溶以及热液演化3个过程中铁同位素地球化学行为的研究现状。

2.1　岩浆演化阶段

源区岩石部分熔融形成岩浆的过程中,由于矿物的熔融顺序以及Fe^{2+}和Fe^{3+}在熔体/固体相间的分配系数不同,熔体相和残留相之间会发生铁同位素分馏(朱祥坤等, 2016)。地幔橄榄岩的主要造岩矿物为橄榄石、斜方辉石、单斜辉石等,部分熔融过程中,单斜辉石首先熔出,其次为斜方辉石,最后是橄榄石,由于单斜辉石和斜方辉石比橄榄石略富集重Fe同位素(图2),所以地幔橄榄岩部分熔融形成的熔体相对残留岩石富集铁的重同位素;同时,Fe^{3+}属

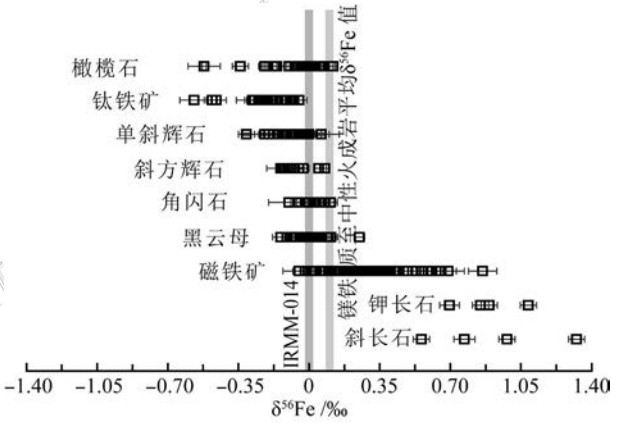

图2　常见岩浆矿物铁同位素组成

数据来源:Beard et al., 2004b; Heimann et al., 2008; Sossi et al., 2012; Telus et al., 2012; Chen et al., 2014; Bilenker et al., 2017; Wu et al., 2017

Fig.2　The iron isotopic composition of common magmatic minerals

Data source: Beard et al., 2004b; Heimann et al., 2008; Sossi et al., 2012; Telus et al., 2012; Chen et al., 2014; Bilenker et al., 2017; Wu et al., 2017

于中等不相容元素，其熔体/固体分配系数约为4.5，而Fe^{2+}的分配系数约为1，意味着部分熔融会导致熔体相比残留相更富集Fe^{3+}（Dauphas et al., 2014），由于Fe^{3+}相对富集铁的重同位素，因而熔融形成的熔体相对残留岩石富集重铁同位素（朱祥坤等，2016）。以上结果显示，岩浆源区氧逸度、部分熔融程度是影响含矿岩浆形成过程中铁同位素分馏的主要因素（Williams et al., 2005; 2014; Dauphas et al., 2009）。

含矿岩浆结晶分异过程中也伴随着铁同位素分馏，主要控制因素为氧逸度和岩浆成分（朱祥坤等, 2016）。不同矿物之间存在明显的铁同位素分馏，铁同位素组成由重到轻变化顺序为：斜长石 > 钾长石 > 磁铁矿 > 黑云母 > 角闪石 > 斜方辉石 > 单斜辉石 > 橄榄石 > 钛铁矿（图2，朱祥坤等，2016），这主要受矿物中Fe^{3+}含量以及Fe-O键能的影响。含矿岩浆演化过程中，具有不同铁同位素组成的矿物从岩浆中分离结晶时，岩浆铁同位素组成会随之变化，如在低氧逸度条件下，橄榄石、辉石等含Fe^{2+}矿物结晶，残余熔体相对富集Fe^{3+}，导致铁的重同位素富集；而在高氧逸度条件下，磁铁矿等含Fe^{3+}的矿物结晶，残余熔体相对富集Fe^{2+}，导致铁的重同位素亏损（朱祥坤等, 2016）。然而，岩浆演化过程中，富集轻铁同位素的矿物（如橄榄石）和富集重铁同位素的矿物（如角闪石）在不同阶段结晶分异，会在一定程度上弱化含矿岩体中的铁同位素分馏现象（Teng et al., 2008; 2013; Schuessler et al., 2009; Du et al., 2017）。

上述研究表明，铁同位素在岩浆起源和演化过程中发生分馏的主要控制因素为氧化还原状态（Fe^{2+}、Fe^{3+}相对比例）。针对花岗岩铁同位素的系统研究显示，还原型花岗岩较氧化型花岗岩富集重铁同位素（Foden et al., 2015）；通过对还原型高温脉状Sn-W矿和氧化型斑岩型Cu-Au矿的对比研究，也证实了岩浆氧化还原状态对铁同位素组成的影响（Wawryk et al., 2015; 2017）。因此，成矿岩体的铁同位素组成被用于反映含矿岩浆的氧化还原状态，西准噶尔包古图被认为是典型的“还原型斑岩铜矿”（Shen et al., 2012; Cao et al., 2016），但是其含矿岩体相对富集铁的轻同位素，指示含矿岩浆为氧化型，其还原特征是次生的，可能是由还原性围岩的混染引起（Zhu et al., 2018），围岩混染改变岩浆铁同位素组成的现象在扬子西缘冷水箐铜镍硫化物矿床中也被报道（Ding et al., 2019）。

2.2 流体出溶阶段

含矿岩浆通过流体出溶完成岩浆到热液过程的过渡，该过程是含矿岩浆能否演化成为岩浆热液矿床的关键（Wilkinson, 2013; Chiaradia, 2014），研究表明，高度演化的酸性岩浆常富集重铁同位素，被认为可能是由于出溶流体带走了轻铁同位素所致（Poitrasson et al., 2005; Heimann et al., 2008）。对众多矽卡岩/斑岩型Cu-Au/Fe矿床的研究，也证实了出溶流体相对于母岩浆富集轻铁同位素的假设（王跃，2011; Zhu et al., 2016; Li et al., 2018; Wang et al., 2021; Zhang et al., 2021）。多个氧化性矽卡岩型和斑岩型矿床（新桥、冬瓜山、凤凰山、张家洼、铁山、Batu Hijau）的Fe同位素研究资料显示，内矽卡岩和磁铁矿相对于成矿岩体富集轻的铁同位素（王跃, 2011; Wawryk et al., 2017; Wang et al., 2021），但不同矿床富集程度不同（图3）。内矽卡岩较轻的铁同位素组成，可能是由铁同位素组成较轻的含矿流体交代成矿岩体所导致（王跃, 2011; Wang et al., 2021）。大部分矽卡岩型矿床（新桥、冬瓜山、霍各乞）表现出围岩相对于岩体和内矽卡岩富集铁的重同位素的特征（王跃, 2011; Pi et al., 2015; Bao et al., 2021），一些矿床（凤凰山、张家洼、邯邢）表现出围岩富集轻铁同位素的特征，但是数据较少，不具参考性。所以，整体可以认为含矿流体富集轻铁同位素这一特征，不是围岩组分的混入造成的。同时，在邯邢与张家洼铁矿床中，蚀变闪长岩的$\delta^{56}Fe$值（−0.071‰~+0.32‰）明显高于未蚀变的闪长岩体（0.01‰~0.04‰），可能反映了在矽卡岩型蚀变过程中，重Fe同位素优先从闪长岩浸出（图3，Zhu et al., 2016, Wang et al., 2021）。综上所述，认为流体从岩体出溶的过程中发生了Fe同位素分馏，相对于岩体，出溶的流体富集轻铁同位素（王跃, 2011; Wang et al., 2021）。磁铁矿沉淀会优先从含矿流体中带走铁的重同位素，因此，其初始成矿流体通常具有较磁铁矿轻的铁同位素组成，磁铁矿的铁同位素组成较成矿岩体轻则可以直接反映成矿流体相比于成矿母岩富集铁的轻同位素（王跃, 2011; Wawryk et al., 2017; Wang et al., 2021）。但是，澳大利亚塔斯马尼亚岛西部的Renison还原性钨-锡矿床中的磁铁矿比其成矿岩体和氧化性斑岩/矽卡岩型矿床的成矿岩体更富集铁的重同位素（图3），因此，认为从相对富集重铁同位素的还原性岩浆中出溶的岩浆热液也

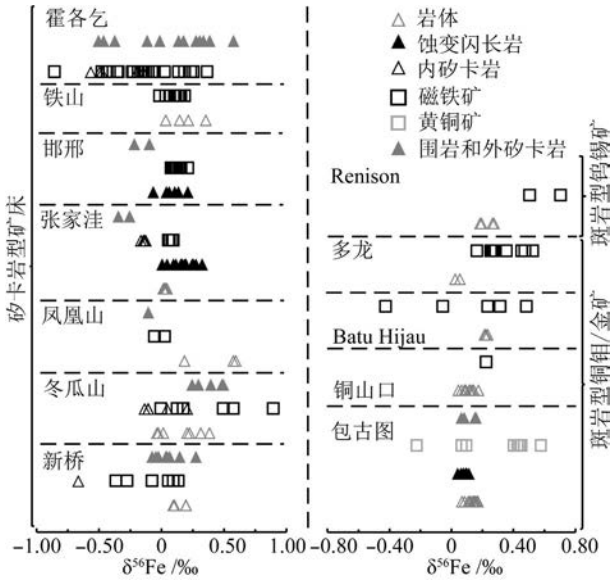

图3　流体出溶过程中相关端员的铁同位素组成

矽卡岩型矿床据王跃, 2011; Pi et al., 2015; Zhu et al., 2016; Bao et al., 2021; Wang et al., 2021; 斑岩型铜钼/金矿床据 Wawryk et al., 2017; Li et al., 2018; Zhu et al., 2018; He et al., 2020; 斑岩型钨锡矿床据 Wawryk et al., 2015

Fig.3　Fe isotope compositions of related end-members in fluid exsolution process

Data of skarn deposits after Wang, 2011; Pi et al., 2015; Zhu et al., 2016; Bao et al., 2021; Wang et al., 2021; Porphyry Cu-Mo/Au deposits after Wawryk et al., 2017; Li et al., 2018; Zhu et al., 2018; He et al., 2020; Porphyry Sn-W deposit after Wawryk et al., 2015

会具有富集重铁同位素的特征(Wawryk et al., 2015)。

通过理论计算获得的成矿流体铁同位素组成,为评价流体出溶过程中熔体-流体间的铁同位素分馏提供了机会。理论计算和实验研究表明,由于流体中的铁元素主要以 $FeCl_2$ 络合物形式溶解,与含 Fe^{3+} 的岩浆相比,会优先富集轻铁同位素(Heimann et al., 2008; Hill et al., 2010; Saunier et al., 2011; Sossi et al., 2017);而当铁元素主要以 $FeCl_4^-$ 形式存在时,出溶流体则富集重铁同位素,因为 $FeCl_4^-$ 中的 Fe 是四面体配位,而熔体中的铁元素是八面体配位(Hill et al., 2010)。出溶流体的铁同位素组成可能受含矿岩浆的氧化还原状态和从流体中沉淀的矿物组合控制,发育磁黄铁矿的还原型矿床的成矿流体富集重铁同位素(Wawryk et al., 2017; Li et al., 2018; Zheng et al., 2021)。此外,在 NaCl-H_2O 体系中进行的相分离实验表明,气相较液相富集重铁同位素(Syverson et al., 2014),说明出溶流体的相分离也会导致铁同位素分馏。以上研究表明,出溶流体和熔体间的铁同位素分馏可能受流体铁的迁移形式、流体出溶程度、熔体的铁同位素组成和氧化还原状态等多种因素控制(Heimann et al., 2008; Dauphas et al., 2017)。

2.3　热液演化阶段

铁作为成矿流体中主要且直接参与成矿的元素,对热液过程中铁同位素的地球化学行为进行研究,可以为反演热液演化过程提供直接约束,进而为成矿过程和矿床成因研究提供关键信息。含矿热液中含铁热液矿物沉淀会引起铁同位素分馏,并最终导致热液的铁同位素随时间演变(Johnson et al., 2002; Welch et al., 2003),如在一些矽卡岩/斑岩型矿床中,随着 Fe^{3+} 矿物(磁铁矿)沉淀,流体逐渐富集轻铁同位素,而随着 Fe^{2+} 矿物(磁黄铁矿)沉淀,流体则逐渐富集重铁同位素(Pi et al., 2015; Wang et al., 2015; Wawryk et al., 2015; Bao et al., 2021)。Wawryk 等(2017)通过典型矿床研究,也提出成矿流体的铁同位素组成主要由流体氧逸度及硫化状态决定的磁黄铁矿(富集轻铁同位素)的沉淀与否控制。共沉淀的含铁矿物之间也存在明显的铁同位素分馏,受控于包括晶体化学、沉淀温度、矿物组合和形成途径在内的多种因素(Rouxel et al., 2008; Syverson et al., 2013, 2017);理论计算和同位素交换实验表明,重铁同位素优先进入含 Fe^{3+}、或者 Fe 占据了化学键最短、最强配位的矿物(Schauble, 2004; Young et al., 2015),同位素平衡条件下,^{56}Fe 富集顺序为黄铁矿>磁铁矿>黄铜矿>菱铁矿~磁黄铁矿(Polyakov et al., 2007; 2011)。然而,在自然热液系统中,由于矿物沉淀过程中铁同位素动力学分馏的存在,如黄铁矿形成过程中,由前驱体 FeS 快速、不可逆沉淀引起的动力学分馏尤为显著(Butler et al., 2005; Guilbaud et al., 2011),导致热液矿物的铁同位素值常具有较大的变化范围(图4)。相比之下,黄铜矿与流体间的铁同位素交换速率快、分馏小,被认为可以有效记录流体的铁同位素组成(Syverson et al., 2017)。因此,在矿床实例研究中,常根据黄铜矿的 $\delta^{56}Fe$ 值和黄铜矿-流体平衡分馏因子,计算成矿流体的 Fe 同位素组成(Li et al., 2018; He et al., 2020)。

不同类型的岩浆热液矿床中含铁热液矿物的铁同位素组成和变化表现出不同的特征(图4),大部分矽卡岩型矿床的含铁矿物表现为更广泛的 $\delta^{56}Fe$ 值

http://www.kcjz.ac.cn

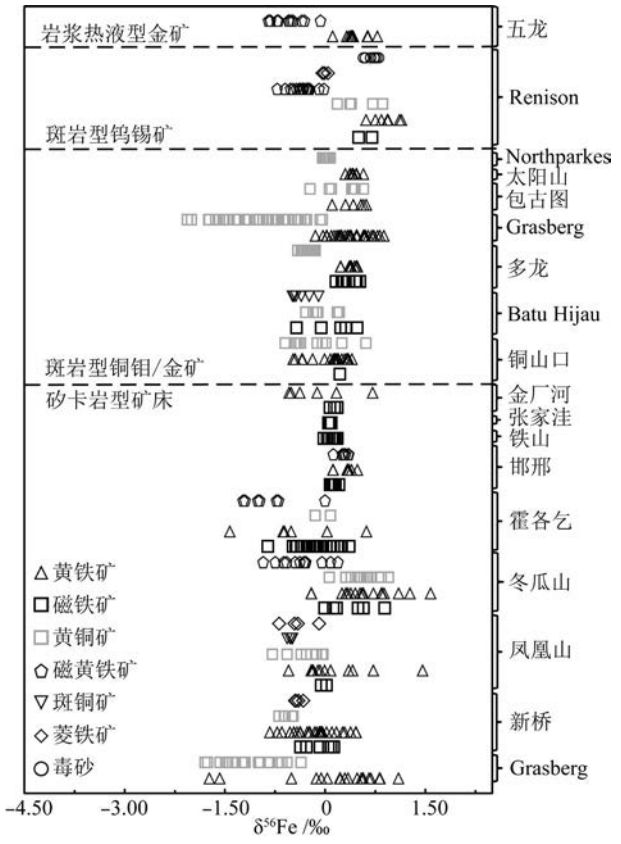

图4 不同岩浆-热液矿床含铁矿物的铁同位素组成

矽卡岩型矿床据Graham et al., 2004; 王跃, 2011; Pi et al., 2015; Zhu et al., 2016; Bao et al., 2021; Wang et al., 2021; 陈福川等, 2022; 斑岩型铜钼/金矿床据Graham et al., 2004; Li et al., 2010; Wawryk et al., 2017; Li et al., 2018; Zhu et al., 2018; He et al., 2020; Zhang et al., 2021; 斑岩型钨锡矿床据Wawryk et al., 2015; 岩浆热液型金矿床据Zheng et al., 2021

Fig.4 Iron isotope composition of iron-bearing minerals in different magmatic-hydrothermal deposits

Data of skarn deposits after Graham et al., 2004; Wang, 2011; Pi et al., 2015; Zhu et al., 2016; Bao et al., 2021; Wang et al., 2021; Chen et al., 2022; Porphyry Cu-Mo/Au deposits after Graham et al., 2004; Li et al., 2010; Wawryk et al., 2017; Li et al., 2018; Zhu et al., 2018; He et al., 2020; Zhang et al., 2021; Porphyry Sn-W deposit after Wawryk et al., 2015; Magmatic hydrothermal gold deposit after Zheng et al., 2021

变化范围(−1.80‰~+1.58‰),同时具有明显的正和负δ^{56}Fe值的偏移(王跃, 2011; Pi et al., 2015; Bao et al., 2021),可能反映了由于低温沉积组分的参与,引起的更复杂的Fe同位素地球化学行为(He et al., 2020)。如中国内蒙古霍各乞矿床中磁铁矿表现出明显的负δ^{56}Fe值(−0.86‰~+0.36‰)(图4),含磁铁矿透闪石岩的δ^{56}Fe值(−0.57‰~−0.15‰)与其围岩(云母片岩、碳质板岩、石英岩)δ^{56}Fe值(−0.12‰~+0.57‰)明显不同,却与碳酸盐岩(−0.51‰~−0.38‰)相一致(图3),推断磁铁矿富轻Fe同位素的特征是成矿流体与碳酸盐岩反应的结果(Bao et al., 2021)。印度尼西亚伊里安查亚省中南部的Grasberg斑岩-矽卡岩型Cu-Au矿床中黄铁矿和黄铜矿的δ^{56}Fe值变化较大(−2.0‰~+1.1‰),被认为是由于沉积铁加入所致(Graham et al., 2004)。其他来自不同斑岩型铜钼/金矿床的含铁氧化物(磁铁矿)和硫化物(黄铁矿、黄铜矿、斑铜矿)表现出基本一致的δ^{56}Fe值变化范围(−0.60‰~+0.61‰, Li et al., 2010; Wawryk et al., 2017; Li et al., 2018; Zhu et al., 2018; He et al., 2020; Zhang et al., 2021),说明斑岩型铜钼/金矿床的热液演化过程中铁同位素的地球化学行为,以及控制铁同位素分馏的主要因素是相似的(He et al., 2020)。与斑岩型铜钼/金矿床相比,斑岩型钨锡矿床中磁铁矿、黄铁矿以及黄铜矿具有更高的δ^{56}Fe值(Wawryk et al., 2015),这种差异是由其中大量磁黄铁矿(富集轻铁同位素)沉淀所引起,可能反映了斑岩型钨锡矿床和斑岩型铜/金矿床成矿流体氧化还原状态的不同(Wawryk et al., 2015; 2017; Li et al., 2018)。五龙岩浆热液型金矿床中磁黄铁矿δ^{56}Fe值变范围−0.85‰~−0.07‰,黄铁矿则为0.11‰~0.78‰,可见磁黄铁矿相对黄铁矿明显富集轻铁同位素,数据表征与理论预测的平衡分馏相一致(Polyakov et al., 2007; 2011)。以上研究结果表明,斑岩型铜钼/金矿床热液矿物δ^{56}Fe值的分布特征,与矽卡岩型和斑岩型钨锡矿床具有明显区别,因此认为Fe同位素在一定程度上能够用于识别斑岩型矿床的矿化类型(He et al., 2020)。

热液演化是时间和空间的函数,通过对不同形成时间、不同空间位置的含铁热液矿物进行Fe同位素组成的综合对比研究,可以获得Fe同位素组成随时间和空间的变化规律(王跃,2011)。含铁热液矿物沉淀会引起铁同位素分馏,并导致成矿热液铁同位素组成随时间演变(Johnson et al., 2002; Welch et al., 2003)。本文将不同岩浆热液矿床中含铁矿物的铁同位素组成按照矿物生成顺序进行了总结,以期定性的反演热液演化过程中Fe同位素随时间的分馏规律(图5)。大部分矿床(新桥、冬瓜山、凤凰山、霍各乞、金厂河、铜山口、Batu Hijau、Renison)中最早期形成的磁铁矿均表现出相对富集重铁同位素的特征;同时,随着热液演化,后期硫化物相对早期硫化物富集重铁同位素;而相对于硫化物,菱铁矿(凤凰

山、Renison)则表现出富轻铁同位素的特征(图5),这说明菱铁矿沉淀时,会优先摄取铁的轻同位素(王跃,2011; Wawryk et al., 2015)。可以发现相对于热液演化最早期形成的磁铁矿,随后形成的硫化物较富集铁的轻同位素;就硫化物而言,热液演化晚期形成的硫化物相对早期硫化物富集铁的重同位素,表现出铁同位素的时间分带性(图5)。

不同空间位置的热液矿物铁同位素组成的对比研究发现,大部分矿床(新桥、冬瓜山、铜山口、Grasberg、五龙)显示出随着含矿流体向远离岩体的迁

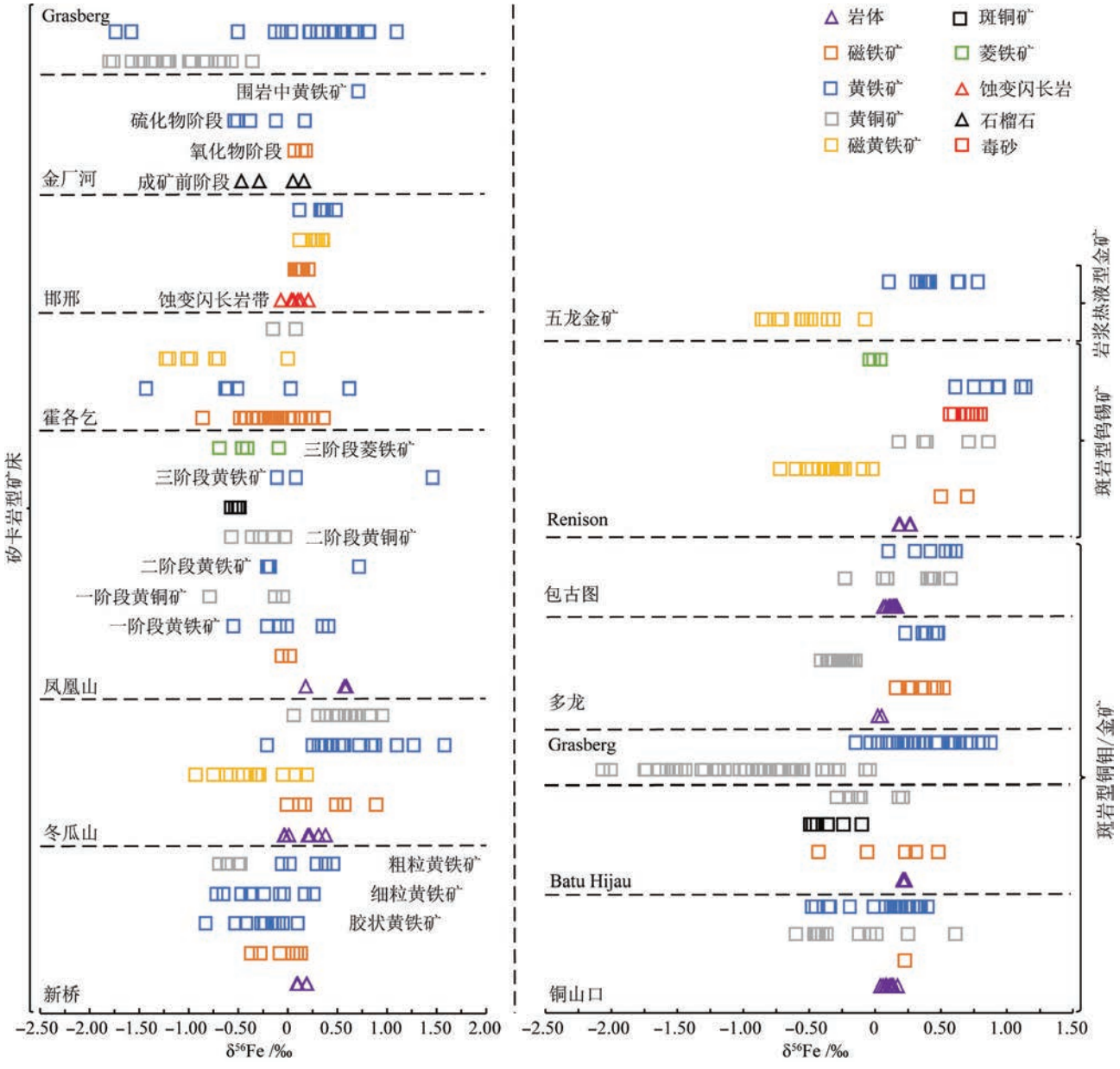

图5　不同岩浆-热液矿床铁同位素组成的时间分带

矽卡岩型矿床据 Graham et al., 2004; 王跃, 2011; Pi et al., 2015; Zhu et al., 2016; Bao et al., 2021; 陈福川等, 2022; 斑岩型铜钼/金矿据 Graham et al., 2004; Wawryk et al., 2017; Li et al., 2018; Zhu et al., 2018; He et al., 2020; 斑岩型钨锡矿据 Wawryk et al., 2015; 岩浆热液型金矿据 Zheng et al., 2021

Fig.5　Time zoning of iron isotopic composition of different magmatic-hydrothermal deposits

Data of skarn deposits after Graham et al., 2004; Wang, 2011; Pi et al., 2015; Zhu et al., 2016; Bao et al., 2021; Chen et al., 2022; Porphyry Cu-Mo/Au deposits after Graham et al., 2004; Wawryk et al., 2017; Li et al., 2018; Zhu et al., 2018; He et al., 2020; Porphyry Sn-W deposit after Wawryk et al., 2015; Magmatic hydrothermal gold deposit after Zheng et al., 2021

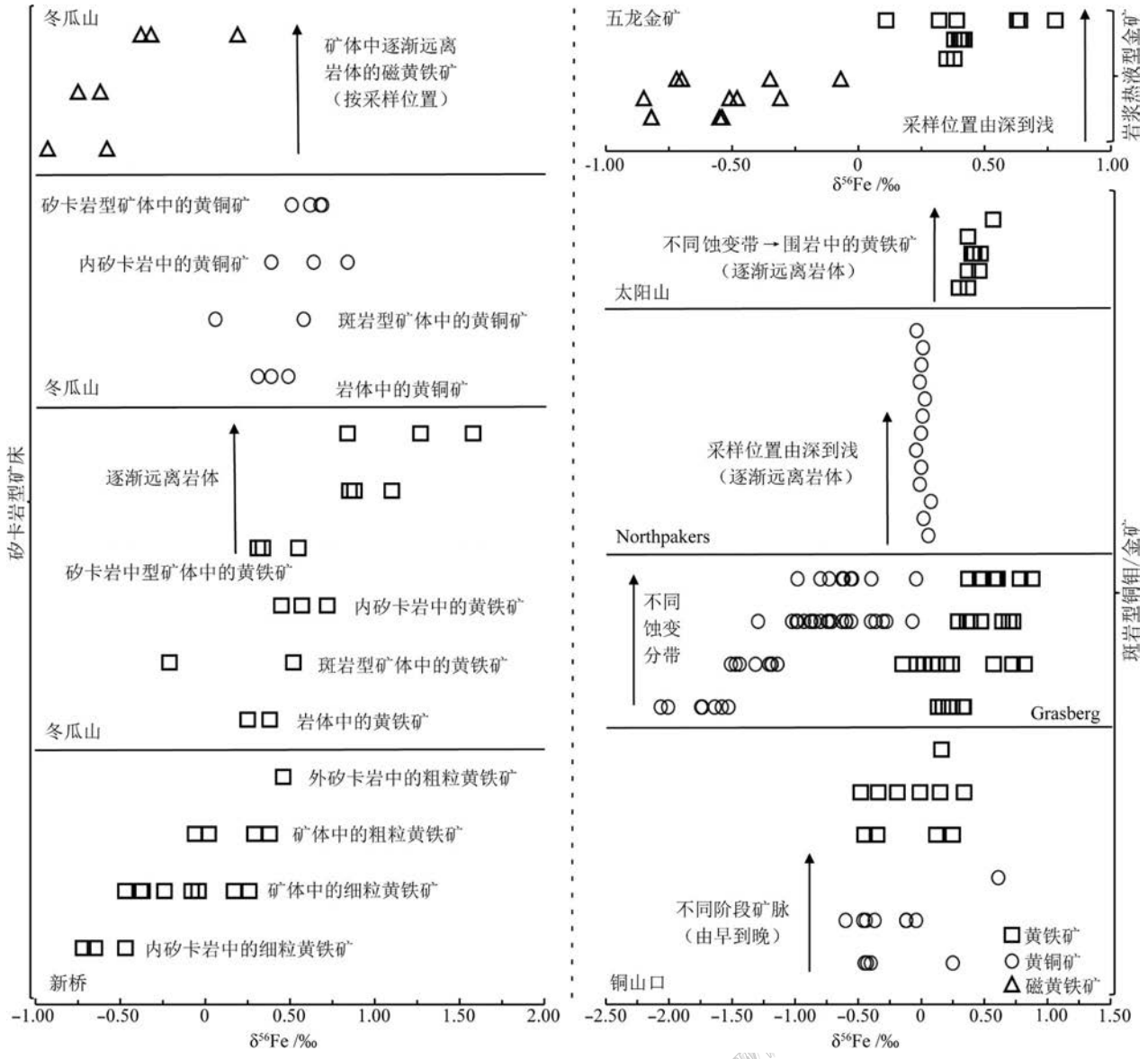

图6 不同岩浆-热液矿床铁同位素组成的空间分带

矽卡岩型矿床据王跃, 2011; 斑岩型铜钼/金矿床据Graham et al., 2004; Li et al., 2010; Zhang et al., 2021; 斑岩型钨锡矿床据Wawryk et al., 2015; 岩浆热液型金矿床据Zheng et al., 2021

Fig.6 Spatial Zoning of iron isotopic composition of different magmatic hydrothermal deposits

Data of skarn deposits after Wang, 2011; Porphyry Cu-Mo/Au deposits after Graham et al., 2004; Li et al., 2010; Zhang et al., 2021; Porphyry Sn-W deposit after Wawryk et al., 2015; Magmatic hydrothermal gold deposit after Zheng et al., 2021

移,热液硫化物的铁同位素组成逐渐变重的特征,铁同位素的空间分带性也非常清晰(图6)。以上铁同位素组成的时空分带性,主要与矿物结晶沉淀引起的铁同位素分馏有关。理论和实验研究表明,热液中迁移的Fe(Ⅲ)相对于Fe(Ⅱ)易于富集铁的重同位素(Johnson et al., 2002; Anbar et al., 2005),热液磁铁矿结晶会优先消耗热液中的重铁同位素,并使得残余流体富集铁的轻同位素,因此,晚于磁铁矿沉淀结晶的硫化物常具有较磁铁矿更轻的铁同位素组成。实验研究表明,在铁元素主要以Fe(Ⅱ)形式迁移的溶液中,硫化物沉淀会优先摄取铁的轻同位素(Butler et al., 2005),因此,随硫化物沉淀,残余热液流体会逐渐富集铁的重同位素,并形成早期硫化物富集轻铁同位素,而晚期硫化物富集重铁同位素的时空分带特征(图5,图6)。但并非所有岩浆热液矿床的热液演化过程中都存在明显的铁同位素分馏并表现

出空间分带性(图6),如澳大利亚Northparkes斑岩型铜金矿床不同深度黄铜矿的$\delta^{56}Fe$值集中于0左右(Li et al., 2010);中国西秦岭太阳山斑岩型铜钼矿床不同蚀变带黄铁矿也无明显分馏($\delta^{56}Fe$=0.30‰~0.57‰,Zhang et al., 2021),导致这种现象的原因还需要进一步的深入研究。

3　铁同位素在岩浆-热液成矿系统中的应用

在已有岩浆-热液成矿系统中Fe同位素地球化学行为研究的基础上,目前铁同位素在岩浆-热液矿床研究中的尝试性应用,主要包括区分成矿热液的氧化还原状态、示踪成矿物质来源两方面。

3.1　铁同位素示踪热液体系氧化还原状态

岩浆-热液成矿系统中铁同位素地球化学行为研究显示,成矿体系的氧化还原状态对含矿岩体和含矿流体的Fe同位素组成起重要的控制作用(Heimann et al., 2008; Dauphas et al., 2017),在此基础上,Li等(2018)探讨了利用铁同位素示踪含矿热液氧化还原状态的可能性,并发现根据黄铜矿的$\delta^{57}Fe$值可以有效区分氧化和还原热液系统(图7)。利用黄铜矿-流体中溶解的$FeCl_4^{2-}$之间的分馏因子,模拟计算了从不同铁同位素组成的流体($\delta^{57}Fe$值范围−1.2‰~1.0‰)中沉淀出的黄铜矿的$\delta^{57}Fe$值(Saunier et al., 2011;Dauphas et al., 2017),将模拟结果与典型还原体系(还原型斑岩铜金矿床、斑岩型钨锡矿床和还原型矽卡岩型铜铁矿床,Wang et al., 2015; Wawryk et al., 2015; Zhu et al., 2018)和氧化体系(氧化型斑岩铜金矿床、浅成低温热液型铜金矿床和氧化型矽卡岩型铜铁矿床,Wang et al., 2011; 2015; Wawryk et al., 2017)中黄铜矿的铁同位素组成进行对比后,发现氧化热液系统中黄铜矿的铁同位素组成明显较还原热液体系轻,由于黄铜矿是岩浆热液矿床中的常见矿物,因此,认为黄铜矿的铁同位素组成可以成为区分热液氧化和还原系统的有效工具(Li et al., 2018)。

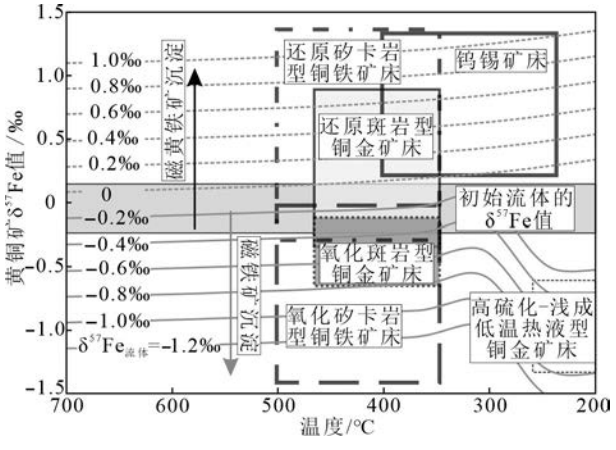

图7　黄铜矿的$\delta^{57}Fe$值与温度关系图(修改自Li et al., 2018)

Fig.7　Relationship between chalcopyrite $\delta^{57}Fe$ value and temperature(modified from Li et al., 2018)

此外,通过对不同类型矿床中黄铁矿和磁黄铁矿铁同位素组成的综合研究,Zheng等(2021)也提出铁同位素可以用于示踪相对还原热液成矿系统中黄铁矿和磁黄铁矿的析出顺序和氧逸度演化趋势。

3.2　铁同位素示踪成矿物质来源

铁元素作为直接参与岩浆热液成矿的元素,其同位素组成的变化规律为直接示踪成矿物质来源提供了可能性。前人通过将成矿体系铁同位素组成与不同储库、与成矿有关地质体以及同类型矿床对比的方法,探讨成矿物质来源(Moeller et al., 2014; Dong et al., 2017; Wang et al., 2017; Rouxel et al., 2018)。如印度尼西亚伊里安查亚省中南部的Grasberg斑岩-矽卡岩型Cu-Au矿床中黄铁矿和黄铜矿的$\delta^{56}Fe$值变化较大(−2.0‰~+1.1‰),被认为是由于沉积铁加入所致(Graham et al., 2004);而澳大利亚新南威尔士州Northparkes斑岩Cu矿中黄铜矿的$\delta^{56}Fe$值集中于0左右,则反映了铁元素单一的岩浆来源(Li et al., 2010);中国西秦岭太阳山斑岩型Cu-Mo矿床含矿斑岩和黄铁矿的铁同位素组成基本一致,表明成矿与含矿斑岩密切相关(Zhang et al., 2021);矽卡岩型矿床中铁同位素组成对比研究表明,流体富集轻铁同位素的特征无法通过围岩组分的加入来解释,表明初始成矿流体来自成矿岩体,矿床中的Fe主要来源于岩浆(王跃, 2011; Zhu et al., 2016; Bao et al., 2021)。以上研究显示,铁同位素可以用于示踪成矿物质来源,然而,流体出溶和演化过程中铁同位素明显的分馏(Wang et al., 2015; Wawryk et al., 2015; Li et al., 2018),导致利用铁同位素示踪成矿物质来源的特殊性。

热液演化过程中,沉淀的矿物组合及其铁同位素组成与热液的氧逸度、硫化状态、温度、压力、络合物成分与含量有关。在详细成矿期次/阶段研究的基础上,进行流体性质、矿物组合和铁同位素组成的

http://www.kcjz.ac.cn/

联合对比研究，可以更有效地示踪成矿物质来源（Wang et al., 2015; Wawryk et al., 2017; He et al., 2020）。铁和硫是许多硫化物中的主要成分，二者的同位素可以在一些相同的过程中发生分馏，例如氧化还原反应（Ohmoto et al., 1982; Field et al., 2005; Dauphas et al., 2017）。由于硫同位素是间接示踪成矿物质来源的成熟传统方法，也常被用于探讨流体性质和演化过程，岩浆-热液成矿系统的成矿温度经历了从高温到低温的演化过程（Sillitoe, 2010; Richards, 2011），并常伴随晚期大气降水的混入，这些因素可能会造成铁同位素的变化不仅仅受控于瑞利分馏，而会出现与成矿环境相关的变化，结合硫同位素可以更有效地示踪成矿物质来源（Hofmann et al., 2009; Gagnevin et al., 2012; Pi et al., 2015）。近年来，有学者尝试将铁、硫同位素联合应用于岩浆-热液成矿系统研究，并提出综合利用铁-硫同位素耦合来示踪成矿物质来源具有极大潜力，例如，将铜山口斑岩铜矿床中含铁矿物的Fe-S同位素组成，与低温非岩浆过程形成的硫化物进行了系统对比，发现高温岩浆热液成因的硫化物显示出相对集中的$\delta^{56}Fe$和$\delta^{34}S$值（图8；He et al., 2020）。

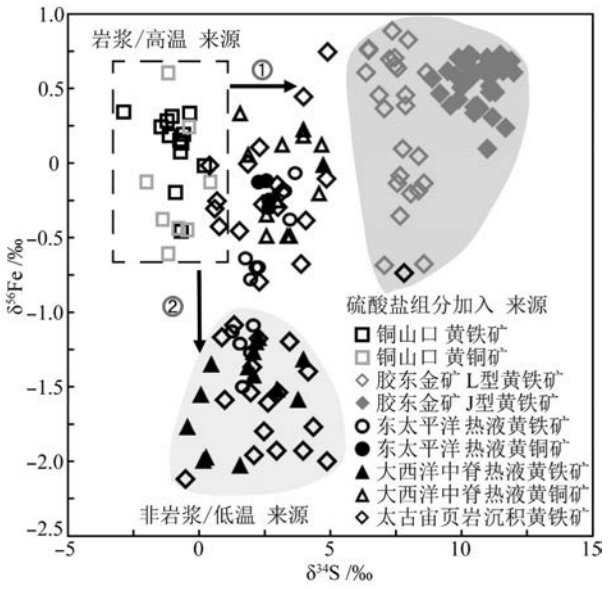

图8 斑岩成矿系统和其他环境中硫化物硫、铁同位素特征对比

①和②分别表示S、Fe同位素分馏过程；铜山口硫化物据He et al., 2020; 胶东金矿硫化物据Zhu et al., 2018; 热液黄铁矿据Rouxel et al., 2004; 2008; 沉积黄铁矿据Marin-Carbonne et al., 2014

Fig.8 Comparison of S and Fe isotope characteristics of sulfides in porphyry metallogenic system and other environments

① and ② represents S and Fe isotope fractionation process respectively; data of Tongshankou sulfide after He et al., 2020; Jiaodong gold deposit sulfide after Zhu et al., 2018; Hydrothermal pyrite after Rouxel et al., 2004; 2008; Sedimentary pyrite after Marin-Carbonne et al., 2014

4 总结和展望

（1）岩浆-热液成矿系统岩浆演化过程中，源区部分熔融和岩浆结晶分异作用都会引起铁同位素分馏，控制分馏的主要因素为源区和岩浆的氧化还原状态（Fe^{2+}、Fe^{3+}相对比例）。

（2）流体出溶过程中也存在铁同位素分馏，在众多矿床中，表现为出溶流体相对于母岩富集轻铁同位素，但理论与实验研究表明出溶流体的铁同位素组成可能受与流体平衡的含Fe^{2+}和Fe^{3+}矿物的比例、流体中铁元素的溶解形式和流体相分离等多个因素影响。

（3）热液演化过程中，随着含铁矿物的结晶沉淀，成矿流体的铁同位素会随之变化，并表现出铁同位素时空分带性，例如，磁铁矿沉淀会导致成矿流体的铁同位素变轻，而磁黄铁矿沉淀则会导致成矿流体的铁同位素组成变重。

（4）由于磁铁矿/磁黄铁矿沉淀对成矿流体铁同位素组成的不同影响，认为黄铜矿的铁同位素组成可用于反映成矿热液体系的氧化还原状态；铁同位素为直接示踪岩浆-热液成矿系统成矿物质来源提供了可能性，但需要在明确不同地质过程中铁同位素分馏机理的基础上进行，铁同位素与硫同位素体系联合应用能更有效的示踪成矿物质来源。

（5）铁同位素在岩浆-热液成矿系统中的研究已经取得了重要进展，未来进一步明确岩浆-热液矿床成矿过程中铁同位素的分馏机理及其控制因素，尝试研究更多岩浆热液矿床的铁同位素组成，扩充矿床学铁同位素数据库，尝试开展铁同位素和其他多种同位素体系的联合应用研究，是对矿床的铁同位素数据做出合理解释，并利用其更有效地示踪成矿过程和成矿物质来源的关键。随着研究的广泛和深入，对岩浆-热液成矿系统乃至其他成矿系统中铁同位素地球化学行为的研究必定会取得更加瞩目的成果。

致 谢 匿名审稿专家和《矿床地质》主编提出的修改意见对于完善本文具有重要帮助，特此感谢。

http://www.kcdz.ac.cn

References

Anbar A D. 2004. Iron stable isotopes: Beyond biosignatures[J]. Earth and Planetary Science Letters, 217(3-4): 223-236.

Anbar A D, Jarzecki A A and Spiro T G. 2005. Theoretical investigation of iron isotope fractionation between $Fe(H_2O)_6^{3+}$ and $Fe(H_2O)_6^{2+}$: Implications for iron stable isotope geochemistry[J]. Geochimica et Cosmochimica Acta, 69(4): 825-837.

Anbar A D and Rouxel O. 2007. Metal stable isotopes in paleoceanography[J]. Annual Review of Earth and Planetary Sciences, 35: 717-746.

Bao C, Zhu X K and Gao Z F. 2021. Iron isotope constraints on the genesis of magnetite ore in the Huogeqi deposit of Inner Mongolia autonomous region in northern China[J]. Ore Geology Reviews, 133: 104116.

Beard B L, Johnson C M, Skulan J L, Nealson K H and Sun H. 2003. Application of Fe isotopes to tracing the geochemical and biological cycling of Fe[J]. Chemical Geology, 195(1): 87-117.

Beard B L and Johnson C M. 2004a. Fe isotope variations in the modern and ancient earth and other planetary bodies[J]. Reviews in Mineralogy and Geochemistry, 55(1):319-357.

Beard B L and Johnson C M. 2004b. Inter-mineral Fe isotope variations in mantle-derived rocks and implications for the Fe geochemical cycle[J]. Geochimica et Cosmochimica Acta, 68(22): 4727-4743.

Bilenker L D, Vantongeren J A, Lundstrom C C and Simon A C. 2017. Iron isotopic evolution during fractional crystallization of the uppermost Bushveld Complex layered mafic intrusion[J]. Geochemistry Geophysics Geosystems, 18(3): 956-972.

Butler I B, Archer C, Vance D, Oldroyd A and Rickard D. 2005. Fe isotope fractionation on FeS formation in ambient aqueous solution[J]. Earth and Planetary Science Letters, 236(1): 430-442.

Cao M J, Qin K Z, Li G M, Evans N J, Hollings P and Jin L J. 2016. Genesis of ilmenite-series I-type granitoids at the Baogutu reduced porphyry Cu deposit, western Junggar, NW-China[J]. Lithos, 246-247: 13-30.

Chen F C, Cheng X L, Han R S, Li G J, Liu J Y, Chang H, Jia Z and Cheng Y. 2022. The fractionation of iron isotope and its constraints on the sources of ore-forming materials in the Jinchanghe skarn polymetallic deposit in Sanjiang region, Southwest China[J]. Acta Petrologica Sinica, 38(1): 157-171(in Chinese with English abstract).

Chen L M, Song X Y, Zhu X K, Zhang X Q, Yu S Y and Yi J N. 2014. Iron isotope fractionation during crystallization and sub-solidus reequilibration: Constraints from the Baima mafic layered intrusion, SW China[J]. Chemical Geology, 380: 97-109.

Cheng Y B, Mao J W, Zhu X K and Wang Y. 2015. Iron isotope fractionation during supergene weathering process and its application to constrain ore genesis in Gaosong deposit, Gejiu district, SW China[J]. Gondwana Research, 27(3): 1283-1291.

Chiaradia M. 2014. Copper enrichment in arc magmas controlled by overriding plate thickness[J]. Nature Geoscience, 7(1): 43-46.

Dauphas N and Rouxel O. 2006. Mass spectrometry and natural variations of iron isotopes[J]. Mass Spectrometry Reviews, 25(5): 831-832.

Dauphas N, Craddock P R, Asimow P D, Bennett V C, Nutman A P and Ohnenstetter D. 2009. Iron isotopes may reveal the redox conditions of mantle melting from Archean to Present[J]. Earth and Planetary Science Letters, 288(1): 255-267

Dauphas N, Roskosz M, Alp E E, Neuville D R, Hu M Y, Sio C K, Tissot Flh, Zhao J, Tissandier L and Médard E. 2014. Magma redox and structural controls on iron isotope variations in Earth's mantle and crust[J]. Earth and Planetary Science Letters, 398: 127-140.

Dauphas N, John S G and Rouxel O. 2017. Iron isotope systematics[J]. Reviews in Mineralogy and Geochemistry, 82(1): 415-510.

Ding X, Ripley E M, Wang W Z, Li C H and Huang F. 2019. Iron isotope fractionation during sulfide liquid segregation and crystallization at the Lengshuiqing Ni-Cu magmatic sulfide deposit, SW China[J]. Geochimica et Cosmochimica Acta, 261: 327-341.

Dong A G, Zhu X K, Li Z H, Kendall B, Li S Z, Wang Y and Tang C. 2017. A multi-isotope approach towards constraining the origin of large-scale Paleoproterozoic B-(Fe) mineralization in NE China[J]. Precambrian Research, 292: 115-129.

Du D H, Wang X L, Yang T, Chen X, Li J Y and Li W Q. 2017. Origin of heavy Fe isotope compositions in high-silica igneous rocks: A rhyolite perspective[J]. Geochimica et Cosmochimica Acta, 218: 58-72.

Field C W, Zhang L, Dilles J H, Rye R O and Reed M H. 2005. Sulfur and oxygen isotopic record in sulfate and sulfide minerals of early, deep, pre-Main Stage porphyry Cu-Mo and Late Main Stage base-metal mineral deposits, Butte district, Montana[J]. Chemical Geology, 215(1): 61-93.

Foden J, Sossi P A and Wawryk C M. 2015. Fe isotopes and the contrasting petrogenesis of A-, I- and S-type granite[J]. Lithos, 212: 32-44.

Gagnevin D, Boyce A J, Barrie C D, Menuge J F and Blakeman R J. 2012. Zn, Fe and S isotope fractionation in a large hydrothermal system[J]. Geochimica et Cosmochimica Acta, 88(7): 183-198.

Gao Z F, Zhu X K, Gao W G, Wang B L, Sun J, Luo Z H, Bao C and Tang C. 2016. Fe isotopic characteristics of the Dongshengmiao and the Tanyaokou polymetallic sulfide deposits in Inner Mongolia and their metallogenic significance[J]. Acta Geologica Sinica, 90(2): 352-360(in Chinese with English abstract).

Gao Z F, Zhu X K, Sun J and Zhou Z L. 2020. Fe-S isotope compositions of the Tanyaokou sulfide deposit in Inner Mongolia and their constraints on sulfide formations[J]. Acta Geoscientica Sinica, 41(5): 675-685(in Chinese with English abstract).

Graham S, Pearson N, Jackson S, Griffin W and O"Reilly S Y. 2004. Tracing Cu and Fe from source to porphyry: In situ determination of Cu and Fe isotope ratios in sulfides from the Grasberg Cu-Au

http://www.kcdz.ac.cn/

deposit[J]. Chemical Geology, 207(3-4): 147-169.

Guilbaud R, Butler I B and Ellam R M. 2011. Abiotic pyrite formation produces a large Fe isotope fractionation[J]. Science, 332(6037): 1548-1551.

He Y S, Hu D P and Zhu C W. 2015. Progress of iron isotope geochemistry in geoscience[J]. Earth Science Frontiers, 22(5): 54-71(in Chinese with English abstract).

He Z W, Zhang X C, Deng X D, Hu H, Li Y, Yu H M, Archer C, Li J W and Huang F. 2020. The behavior of Fe and S isotopes in porphyry copper systems: Constraints from the Tongshankou Cu-Mo deposit, eastern China[J]. Geochimica et Cosmochimica Acta, 270: 61-83.

Heimann A, Beard B L and Johnson C M. 2008. The role of volatile exsolution and sub-solidus fluid/rock interactions in producing high Fe-56/Fe-54 ratios in siliceous igneous rocks[J]. Geochimica et Cosmochimica Acta, 72(17): 4379-4396.

Hill P S, Schauble E A and Young E D. 2010. Effects of changing solution chemistry on Fe^{3+}/Fe^{2+} isotope fractionation in aqueous Fe-Cl solutions[J]. Geochimica et Cosmochimica Acta, 74(23): 6669-6689.

Hofmann A, Bekker A, Rouxel O, Rumble D and Master S. 2009. Multiple sulphur and iron isotope composition of detrital pyrite in Archaean sedimentary rocks: A new tool for provenance analysis[J]. Earth and Planetary Science Letters, 286(3): 436-445.

Huang Q Y, Viehmann S, Walde D H G and Li W Q. 2021. Iron isotope constraints on the metal source and depositional environment of the Neoproterozoic banded iron- and manganese deposits in Urucum, Brazil[J]. Geochemistry, 81(3): 125771.

Johnson C M, Skulan J L, Beard B L, Sun H, Nealson K H and Braterman P S. 2002. Isotopic fractionation between Fe(Ⅲ) and Fe(Ⅱ) in aqueous solutions[J]. Earth and Planetary Science Letters, 195 (1): 141-153.

Johnson C M, Beard B L and Roden E E. 2008. The iron isotope fingerprints of redox and biogeochemical cycling in the modern and ancient Earth[J]. Annual Review of Earth and Planetary Sciences, 36 (1): 457-493.

Li J X, Qin K Z, Li G M, Noreen J E, Huang F and Zhao J X. 2018. Iron isotope fractionation during magmatic-hydrothermal evolution: A case study from the Duolong porphyry Cu-Au deposit, Tibet[J]. Geochimica et Cosmochimica Acta, 238: 1-15.

Li Q W, Zhao J H, Wang Q, Zhang Z F, An Y J and He Y T. 2020. Iron isotope fractionation in hydrous basaltic magmas in deep crustal hot zones[J]. Geochimica et Cosmochimica Acta, 279: 29-44.

Li W Q, Jackson S E, Pearson N J and Graham S. 2010. Copper isotopic zonation in the Northparkes porphyry Cu-Au deposit, SE Australia[J]. Geochimica et Cosmochimica Acta, 74: 4078-4096.

Li W Q, Huberty J M, Beard B L, Kita N T, Valley J W and Johnson C M. 2013. Contrasting behavior of oxygen and iron isotopes in banded iron formations revealed by in situ isotopic analysis[J]. Earth and Planetary Science Letters, 384: 132-143.

Liu C H, Liu J J, Carranza M J E, Wang J P, Zhai D G, Zhang F F, Wang Y H and Liu Z J. 2021. Iron and magnesium isotope systematics from the Shuangwang gold deposit in the Qinling orogen, Central China[J]. Ore Geology Reviews, 134: 104123.

Liu P P, Zhou M F, Luais B, Cividini D and Bard C R. 2014. Disequilibrium iron isotopic fractionation during the high-temperature magmatic differentiation of the Baima Fe-Ti oxide-bearing mafic intrusion, SW China[J]. Earth and Planetary Science Letters, 399: 21-29.

Marin C J, Rollion B C, Bekker A, Rouxel O, Agangi A, Cavalazzi B, Wohlgemuth-Ueberwasser C C, Hofmann A and Mckeegan K D. 2014. Coupled Fe and S isotope variations in pyrite nodules from Archean shale[J]. Earth and Planetary Science Letters, 392: 67-79.

Moeller K, Schoenberg R, Grenne T, Thorseth I H, Drost K and Pedersen R B. 2014. Comparison of iron isotope variations in modern and Ordovician siliceous Fe oxyhydroxide deposits[J]. Geochimica et Cosmochimica Acta, 126: 422-440.

Ohmoto H and Lasaga A C. 1982. Kinetics of reactions between aqueous sulfates and sulfides in hydrothermal systems[J]. Geochimica et Cosmochimica Acta, 46(10): 1727-1745.

Pi Q H, Zhong R C and Hu R Z. 2015. Tracing the ore-formation history of the shear-zone-controlled Huogeqi Cu-Pb-Zn deposit in Inner Mongolia, northern China, using H, O, S, and Fe isotopes[J]. Ore Geology Reviews, 71: 263-272.

Poitrasson F and Freydier R. 2005. Heavy iron isotope composition of granites determined by high resolution MC-ICP-MS[J]. Chemical Geology, 222(1-2): 132-147.

Polyakov V B, Clayton R N, Horita J and Mineev S D. 2007. Equilibrium iron isotope fractionation factors of minerals: Reevaluation from the data of nuclear inelastic resonant X-ray scattering and Mössbauer spectroscopy[J]. Geochimica et Cosmochimica Acta, 71 (15): 3833-3846.

Polyakov V B and Soultanov D M. 2011. New data on equilibrium iron isotope fractionation among sulfides: Constraints on mechanisms of sulfide formation in hydrothermal and igneous systems[J]. Geochimica et Cosmochimica Acta, 75(7): 1957-1974..

Richards J P. 2011. Magmatic to hydrothermal metal fluxes in convergent and collided margins[J]. Ore Geology Reviews, 40(1): 1-26.

Rouxel O, Fouquet Y and Ludden J N. 2004. Subsurface processes at the lucky strike hydrothermal field, Mid-Atlantic ridge: Evidence from sulfur, selenium, and iron isotopes[J]. Geochimica et Cosmochimica Acta, 68(10): 2295-2311.

Rouxel O, Shanks W C, Bach W and Edwards K J. 2008. Integrated Fe- and S-isotope study of seafloor hydrothermal vents at East Pacific Rise 9~10°N[J]. Chemical Geology, 252(3): 214-227.

Rouxel O, Toner B, Germain Y and Glazer B. 2018. Geochemical and iron isotopic insights into hydrothermal iron oxyhydroxide deposit formation at Loihi Seamount[J]. Geochimica et Cosmochimica Acta, 220: 449-482.

Saunier G, Pokrovski G S and Poitrasson F. 2011. First experimental determination of iron isotope fractionation between hematite and aqueous solution at hydrothermal conditions[J]. Geochimica et

http://www.kcdz.ac.cn/

Cosmochimica Acta, 75(21): 6629-6654.

Schauble E A. 2004. Applying stable isotope fractionation theory to new systems[J]. Reviews in Mineralogy and Geochemistry, 55(1): 65-111.

Schuessler J A, Schoenberg R and Sigmarsson O. 2009. Iron and lithium isotope systematics of the Hekla volcano, Iceland: Evidence for Fe isotope fractionation during magma differentiation[J]. Chemical Geology, 258(1-2): 78-91.

Shen P, Shen Y C, Pan H D, Li X H, Dong L H, Wang J B, Zhu H P, Dai H W and Guan W N. 2012. Geochronology and isotope geochemistry of the Baogutu porphyry copper deposit in the West Junggar region, Xinjiang, China[J]. Journal of Asian Earth Sciences, 49: 99-115.

Shen P and Pan H D. 2015. Methane origin and oxygen-fugacity evolution of the Baogutu reduced porphyry Cu deposit in the West Junggar terrain, China[J]. Mineralium Deposita, 50(8): 967-986.

Sillitoe R H. 2010. Porphyry copper systems[J]. Econ. Geol., 105(1): 3-41.

Sossi P A, Foden J D and Halverson G P. 2012. Redox-controlled iron isotope fractionation during magmatic differentiation: An example from the Red Hill intrusion, S. Tasmania[J]. Contributions to Mineralogy and Petrology, 164(5): 757-772.

Sossi P A and O'neill H S C. 2017. The effect of bonding environment on iron isotope fractionation between minerals at high temperature[J]. Geochimica et Cosmochimica Acta, 196: 121-143.

Sun W D, Huang R F, Li H, Hu Y B, Zhang C C, Sun S J, Zhang L P, Ding X, Li C Y, Zartman R E and Ling M X. 2015. Porphyry deposits and oxidized magmas[J]. Ore Geology Reviews, 65: 97-131.

Syverson D D, Borrok D M and Seyfried W E. 2013. Experimental determination of equilibrium Fe isotopic fractionation between pyrite and dissolved Fe under hydrothermal conditions[J]. Geochimica et Cosmochimica Acta, 122: 170-183.

Syverson D D, Pester N J, Craddock P R and Seyfried W E J. 2014. Fe isotope fractionation during phase separation in the NaCl-H_2O system: An experimental study with implications for seafloor hydrothermal vents[J]. Earth and Planetary Science Letters, 406: 223-232.

Syverson D D, Luhmann A J, Tan C Y, Borrok D M, Ding K and Seyfried W E. 2017. Fe isotope fractionation between chalcopyrite and dissolved Fe during hydrothermal recrystallization: An experimental study at 350°C and 500 bars[J]. Geochimica et Cosmochimica Acta, 200: 87-109.

Telus M, Dauphas N, Moynier F, Tissot F L H, Teng F Z, Nabelek P I, Craddock P R and Groat L A. 2012. Iron, zinc, magnesium and uranium isotopic fractionation during continental crust differentiation: The tale from migmatites, granitoids, and pegmatites[J]. Geochimica et Cosmochimica Acta, 97: 247-265.

Teng F Z, Dauphas N and Helz R T. 2008. Iron isotope fractionation during magmatic differentiation in Kilauea Iki Lava Lake[J]. Science, 320(5883): 1620-1622.

Teng F Z, Dauphas N, Huang S and Marty B. 2013. Iron isotopic systematics of oceanic basalts[J]. Geochimica et Cosmochimica Acta, 107: 12-16.

Troll V R, Weis F A, Jonsson E, Andersson U B, Majidi S A, Hogdahl K, Harris C, Millet M, Chinnasamy S S, Kooijman E and Nilsson K P. 2019. Global Fe-O isotope correlation reveals magmatic origin of Kiruna-type apatite-iron-oxide ores[J]. Nature Communications, 10(1): 1712-1724.

Wang D, Sun X, Zheng Y Y, Wu S, Xia S L, Chang H F and Yu M. 2017. Two pulses of mineralization and genesis of the Zhaxikang Sb-Pb-Zn-Ag deposit in southern Tibet: Constraints from Fe-Zn isotopes[J]. Ore Geology Reviews, 84: 347-363.

Wang S J, Sun W D, Huang J, Zhai S K and Li H M. 2020. Coupled Fe-S isotope composition of sulfide chimneys dominated by temperature heterogeneity in seafloor hydrothermal systems[J]. Science Bulletin, 65(20): 1767-1774.

Wang Y. 2011. Fe and Cu isotopic geochemistry in Tongling ore concentration area[D]. Beijing: Chinese Academy of Geological Sciences. 128p(in Chinese with English abstract).

Wang Y, Zhu X K, Mao J W, Li Z H and Cheng Y B. 2011. Iron isotope fractionation during skarn-type metallogeny: A case study of Xinqiao Cu-S-Fe-Au deposit in the Middle-Lower Yangtze valley[J]. Ore Geology Reviews, 43(1): 194-202.

Wang Y and Zhu X K. 2012. Fe isotope systematics and its implications in ore deposit geology[J]. Acta Petrologica Sinica, 28(11): 3638-3654(in Chinese with English abstract).

Wang Y, Zhu X K and Cheng Y B. 2015. Fe isotope behaviours during sulfide-dominated skarn-type mineralisation[J]. Journal of Asian Earth Sciences, 103: 374-392.

Wang Y, Zhu X K, Tang C, Mao J W and Chang Z S. 2021. Discriminate between magmatic- and magmatic-hydrothermal ore deposits using Fe isotopes[J]. Ore Geology Reviews, 130: 103946.

Wawryk C M and Foden J D. 2015. Fe-isotope fractionation in magmatic-hydrothermal mineral deposits: A case study from the Renison Sn-W deposit, Tasmania[J]. Geochimica et Cosmochimica Acta, 150: 285-298.

Wawryk C M and Foden J D. 2017. Iron-isotope systematics from the Batu Hijau Cu-Au deposit, Sumbawa, Indonesia[J]. Chemical Geology, 466: 159-172.

Wei G J, Huang F, Ma J L, Deng W F, Yu H M, Kang J T and Chen X F. 2022. Progress of Non-traditional stable isotope geochemistry of the past decade in China[J]. Bulletin of Mineralogy Petrology and Geochemistry, 41(1): 1-44(in Chinese with English abstract).

Welch S A, Beard B L, Johnson C M and Braterman P S. 2003. Kinetic and equilibrium Fe isotope fractionation between aqueous Fe(Ⅱ) and Fe(Ⅲ)[J]. Geochimica et Cosmochimica Acta, 67(22): 4231-4250.

Wilkinson J J. 2013. Triggers for the formation of porphyry ore deposits in magmatic arcs[J]. Nature Geoscience, 6(11): 917-925.

Williams H M, Peslier A. H, Mccammon C, Halliday A N, Levasseur S, Teutsch N and Burg J P. 2005. Systematic iron isotope variations in mantle rocks and minerals: The effects of partial melting

http://www.kcdz.ac.cn/

and oxygen fugacity[J]. Earth and Planetary Science Letters, 235 (1): 435-452.

Williams H M and Bizimis M. 2014. Iron isotope tracing of mantle heterogeneity within the source regions of oceanic basalts[J]. Earth and Planetary Science Letters, 404: 396-407.

Wu H J, He Y S, Bao L E, Zhu C W and Li S G. 2017. Mineral composition control on inter-mineral iron isotopic fractionation in granitoids[J]. Geochimica et Cosmochimica Acta, 198: 208-217.

Xiang L, Schoepfer S D, Zhang H, Chen Z W, Cao C Q and Shen S Z. 2020. Deep-water dissolved iron cycling and reservoir size across the Ediacaran-Cambrian transition[J]. Chemical Geology, 541: 119575.

Yang X Q, Mao J W, Jiang Z S, Santosh M, Zhang Z H, Duan S G and Wang D C. 2019. The Carboniferous Shikebutai iron deposit in Western Tianshan, Northwestern China: Petrology, Fe-O-C-Si isotopes, and implications for iron pathways[J]. Econ. Geol., 114(6): 1207-1222.

Young E D, Manning C E, Schauble E A, Shahar A, Macris C A, Lazar C and Jordan M. 2015. High-temperature equilibrium isotope fractionation of non-traditional stable isotopes: Experiments, theory, and applications[J]. Chemical Geology, 395: 176-195.

Zhang L, Qiu K F, Hou Z L, Franco P, Espine S and Cai Y W. 2021. Fluid-rock reactions of the Triassic Taiyangshan porphyry Cu-Mo deposit(West Qinling, China) constrained by QEMSCAN and iron isotope[J]. Ore Geology Reviews, 132: 104068.

Zhang Y W, Fan H R, Hu F F, Liu X, Xie L W and Li X H. 2021. Extreme iron isotope variation of pyrite in the Muping gold deposit, Jiaodong: Implication for tracing metal origin[J]. Ore Geology Reviews, 139: 104431.

Zheng J H, Chen B, Liu S J and Bao C. 2021. Iron isotope fractionation in reduced hydrothermal gold deposits: A case study of the Wulong gold deposit, Liaodong Peninsula, East China[J]. American Mineralogist, 106(3): 430-442.

Zhu B, Zhang H F, Zhao X M and He Y S. 2016. Iron isotope fractionation during skarn-type alteration: Implications for metal source in the Han-Xing iron skarn deposit[J]. Ore Geology Reviews, 74: 139-150.

Zhu B, Zhang H F, Shen P, Su B X, Xiao Y and He Y S. 2018. Redox state of the Baogutu reduced porphyry Cu deposit in the Central Asian Orogenic belt[J]. Ore Geology Reviews, 101: 803-818.

Zhu X K, O'nions R K, Guo Y L and Reynolds B C. 2000. Secular variation of iron isotopes in North Atlantic deep water[J]. Science, 287 (17): 2000-2002.

Zhu X K, Sun J and Wang Y. 2016. The geochemistry behavior of iron isotopes in magma processes[J]. Journal of Earth Sciences and Environment, 38(1):1-10(in Chinese with English abstract).

Zhu X K, Sun J and Li Z H. 2019. Iron isotopic variations of the Cryogenian banded iron formations: A new model[J]. Precambrian Research, 331: 105359.

Zhu Z Y, Jiang S Y, Mathur R, Cook N J, Yang T, Wang M, Ma L and Ciobanu C L. 2018. Iron isotope behavior during fluid/rock interaction in K-feldspar alteration zone——A model for pyrite in gold deposits from the Jiaodong Peninsula, East China[J]. Geochimica et Cosmochimica Acta, 222: 94-116.

附中文参考文献

陈福川, 程晓林, 韩润生, 李龚健, 刘金宇, 常河, 贾祯, 程岩. 2022. 西南三江金厂河矽卡岩型多金属矿床铁同位素分馏机制及其对成矿物质来源的制约[J]. 岩石学报, 38: 157-171.

高兆富, 朱祥坤, 高文革, 王炳林, 孙剑, 罗照华, 包创, 唐超. 2016. 内蒙古东升庙和炭窑口多金属硫化物矿床铁同位素地球化学特征及其成矿指示意义[J]. 地质学报, 90(2): 352-360.

高兆富, 朱祥坤, 孙剑, 周子龙. 2020. 内蒙古炭窑口硫化物矿床Fe、S同位素组成及对硫化物成矿的制约[J]. 地球学报, 41(5): 675-685.

何永胜, 胡东平, 朱传卫. 2015. 地球科学中铁同位素研究进展[J]. 地学前缘, 22(5): 54-71.

王跃. 2011. 铜陵矿集区Fe、Cu同位素地球化学研究[D]. 北京：中国地质科学院. 128页.

王跃, 朱祥坤. 2012. 铁同位素体系及其在矿床学中的应用[J]. 岩石学报, 28: 3638-3654.

韦刚健, 黄方, 马金龙, 邓文峰, 于慧敏, 康晋霆, 陈雪霏. 2022. 近十年中国非传统稳定同位素地球化学研究进展[J]. 矿物岩石地球化学通报, 41(1): 1-44.

朱祥坤, 孙剑, 王跃. 2016. 岩浆过程中铁同位素的地球化学行为[J]. 地球科学与环境学报, 38: 1-10.

http://www.ncdz.ac.cn